 CMC, vol.2, no.1, pp.39-49, 2005

Numerical Analysis of Parameters in a Laminated Beam Model by Radial Basis Functions

Y. C. Hon[1] , **L. Ling**[2] **and K. M. Liew**[3]

Abstract: In this paper we investigate a thermal driven Micro-Electrical-Mechanical system which was originally designed for inkjet printer to precisely deliver small ink droplets onto paper. In the model, a tiny free-ended beam of metal bends and projects ink onto paper. The model is solved by using the recently developed radial basis functions method. We establish the accuracy of the proposed approach by comparing the numerical results with reported experimental data. Numerical simulations indicate that a light (low composite mass) beam is more stable as it does not oscillate much. A soft (low rigidity) beam results in a higher rate of deflection, when compared to a high rigidity one. Effects caused by the values of physical parameters are also studied. Finally, we give a prediction on the optimal time for the second current pulse which results in maximum rate of second deflection of the beam.

keyword: Micro-Electrical-Mechanical system, Thermal driven, Radial Basis Functions method

1 Introduction

Micro-Electro-Mechanical-System (MEMS) is an integration of mechanical elements, sensors, actuators, and electronics on a common silicon substrate through the utilization of micro-fabrication technology. The dimensions of MEMS devices are usually in micrometer scale whose design and manufacturing processes require the use of electrically-driven motors smaller than the diameter of a human hair. Studies of the complicated mechanical, thermal, biological, chemical, optical, and magnetic phenomena are particularly challenging for quantitative analyses and modelling. During the last decade, intensive research studies in MEMS have enabled many fruitful developments in the design, construction, and fabrication of the MEMS devices. For instance, the micro-accelerometer for crash air-bag deployment system and the active suspension system for automobiles; the micro-valves, micro-pumps and micro-actuators for fluidic transport, mixing and particle filtering; the micro-mirror switches and the snapping micro-switches for radio frequency have increased tremendously the portability and applicability of electronic and electrical products; and the human blood pressure monitors and the polymer micro-fluidic chips have been widely adopted for medical diagnostics and drug discovery.

The main structure of many components like micro switches and micro mirrors can be simplified as a 1D-beam or a 2D-plate mode which consists of fourth-order differential equations. To further simplify the model, Huang, Liew, and et al. (2001) used a lumped model composed of mass, spring and damp to study the beam structure (called ”bridge”) in the micro switch. In their work they designed a static electromechanical model for the residual stress effect to predict the stiffness and pull-in voltage. They also used a nonlinear dynamic model that captured the essential characteristics of the bridge to predict the switching speed and the Q-factor. Younis, Abdel-Rahman, and Nayfeh (2003) proposed a macro model for microbeam-based MEMS by discretizing the distributed-parameter system using a Galerkin procedure into a finite-degree-of-freedom system, consisting of ordinary differential equations (ODEs) in time. Their model considered moderately large deflections, dynamics loads and coupling between mechanical and electrical forces. The model successfully predicted the pull-in voltage, natural frequencies and pull-in time. Bochobza-Degani and Nemirovsky (2002) proposed a pull-in model of two degrees of freedom to model the pull-in parameters of electrostatic actuators. Their model is more accurate than the traditional one-degree-of-freedom one. On the topic of system-level simulation, Endemano,

[1] City University of Hong Kong, Hong Kong. The work described in this paper was fully supported by a grant from the Research Grants Council of the Hong Kong Special Administrative Region, China (Project No. CityU 1185/03E).

[2] City University of Hong Kong, Hong Kong

[3] Nanyang Technological University, Singapore

Desmuillez, and Dunnigan (2002) proposed an analytical torque model to describe the electrostatic actuator. The model is included into system level simulation of a micromotor by hardware description language-analogue mixed signal (VHDL-AMS).

Most MEMS models require solving differential equation in several coupled energy domains and complicated actuation mechanism. Due to the lack of suitable numerical and analytical methods, most of the MEMS design processes, however, are still performed in a primitive trial-and-error fashion. These methods normally require several modifications before MEMS devices are finally modeled. This results in an inefficient and ineffective production cycle for commercial product development. Developments in advanced numerical techniques and simulation tools will definitely be beneficial to MEMS design and production processes.

Numerical modeling and simulation for MEMS devices involve knowledge of various disciplines such as mechanical, thermal, fluidic, electrical, magnetic, chemical and optical engineering. Recently, the development of Nano-Electro-Mechanical systems (NEMS), which are thousand times smaller than MEMS, has given a significant impact on medical, automobile, aerospace and information technology areas [Kovacs (1998)]. Some prospective applications of NEMS include random access memory [Rueckes, Kim, Joselevich, Tseng, Cheung, and Lieber (2000)], super-sensitive sensors [Collins, Bradley, Ishigami, and Zettl (2000)], and nano-tweezers for miniaturized robotics [Kim and Lieber (1999)].

This paper is organized as follows: In Section 2, the physical beam model is stated. The numerical formulation for solving the model will be given in Section 3. Numerical results are then given in Section 4 to verify the efficiency and accuracy of the proposed method.

2 Physical Model

A beam composed of two materials, aluminum (Al) and silicon dioxide (SiO_2) in a ratio of 2:3, was manufactured at Eastman Kodak with the overall dimensions $100\mu\text{m} \times 20\mu\text{m} \times 50\mu\text{m}$, see Figure 1. A voltage pulse of 10μs was applied to the beam heating it up to about 400K and resulting in a maximum rate of deflection of about 0.2ms^{-1}.

The model of this problem is divided into two main parts:

Heat Transport Due to the difference in thermal expansion coefficient of Al and SiO_2, the laminated beam will bend when a current is supplied. This generates a certain amount of heat.

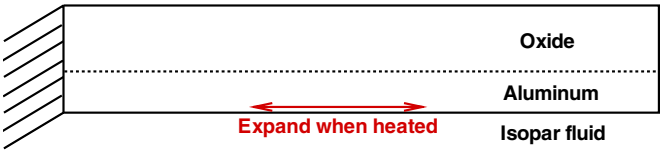

Figure 1 : Laminated beam model.

Beam Fluid Interaction When the beam is heated, its motion is governed by a beam equation that satisfies a total effective moment condition. The motion is linear with respect to the applied temperature, at the free end.

The model of the laminated beam was given in [Ross, Biswanger, Bohun, Bridge, Ling, Noel, Saujani, Spirn, and Ting (2000)] as follow:

The equations governing the heat flow are:

$$\begin{aligned} \text{Isopar Fluid:} \quad & \rho_f c_{v_f} \frac{\partial u}{\partial t} = k_f \frac{\partial^2 u}{\partial x^2}, \\ \text{Silicon Oxide:} \quad & \rho_{\text{ox}} c_{v_{\text{ox}}} \frac{\partial u}{\partial t} = k_{\text{ox}} \frac{\partial^2 u}{\partial x^2}, \\ \text{Aluminum:} \quad & \rho_{\text{Al}} c_{v_{\text{Al}}} \frac{\partial u}{\partial t} = k_{\text{Al}} \frac{\partial^2 u}{\partial x^2} + Q. \end{aligned} \tag{1}$$

Some of the thermal properties of Al, SiO_2 and surrounding Isopar fluid[4] is listed in Table 1. The boundary conditions are determined by the empirical fact that temperature is continuous and energy is conserved across the interface boundaries. These conditions imply

$$\begin{aligned} \theta(\text{interface}^-) &= \theta(\text{interface}^+), \\ k^- \frac{\partial u}{\partial x}(\text{interface}^-) &= k^+ \frac{\partial u}{\partial x}(\text{interface}^+), \end{aligned} \tag{2}$$

at any interface. In addition, the boundary conditions at infinity are given to be room temperature $\theta(x = \pm\infty,\, t) = 300\text{K}$. For a $10\mu s$ heating pulse, the resulting temperature profiles are displayed in Figure 2. Since the conductivity

[4] Isopar is the brand name for a synthetically produced Isoparaffinic fluid. Isopar fluids have exceptionally high purity and uniform composition. They are available in a wide range of evaporation rates. Processing is stringently controlled to provide products with extremely low odor, selective solvency, excellent stability, and narrow distillation ranges.

k of aluminum is so high, it can be assumed that the temperature variation across the aluminum is zero and the temperature of aluminum is spatially uniform. The temperature of the aluminum layer, θ_{Al} in Figure 2(b), is of central importance in the second part of this model.

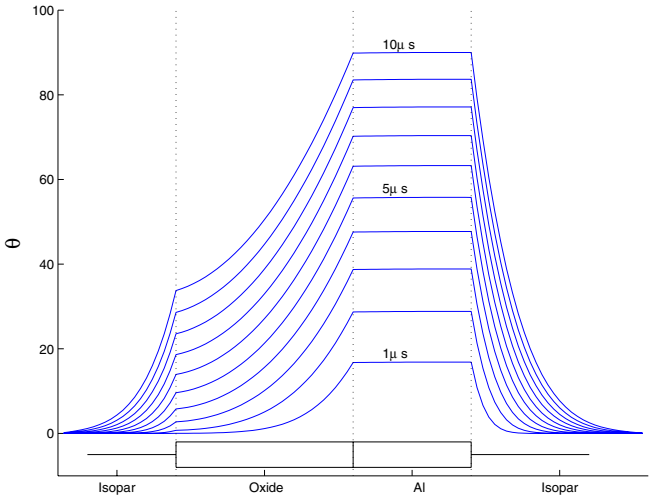

(a) Cross section of the beam.

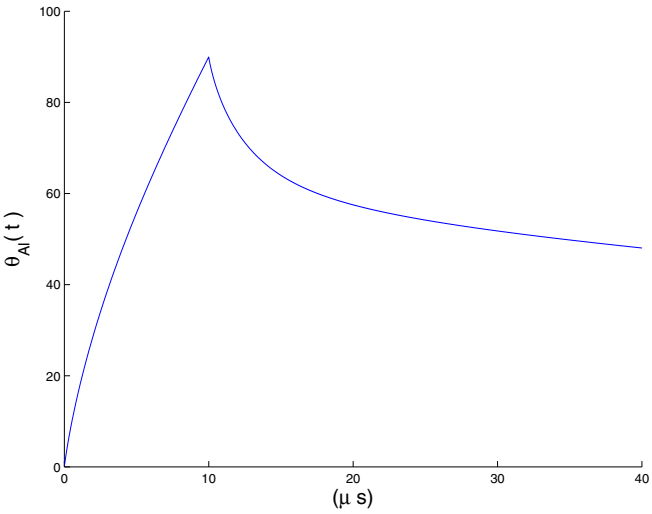

(b) Average temperature of the Al layer.

Figure 2 : Temperature profile as a $10\mu s$ heating pulse is applied.

The motion of the beam is governed by the beam equation with both the drag and the viscosity of the fluid taken into account,

$$(\beta+\rho H)\frac{\partial^2 u}{\partial t^2} = -D\frac{\partial^4 u}{\partial x^4} - k\frac{\partial u}{\partial t},\ x\in[0,L],\ t\in[0,T], \quad (3)$$

Material	ρ (g cm^{-2})	c_v (Jg^{-1}K^{-1})	k (Jcm^{-1}s^{-1}K^{-1})
Isopar Fluid	0.77	2.1	$1E-3$
Silicon Dioxide	3.4	0.7	$1.38E-2$
Aluminum	2.7	0.5	2.31

Table 1 : Thermal properties of Al, SiO_2 and surrounding Isopar fluid.

where ρ is the weighted density, D is the composite flexural rigidity, P is the external pressure, H is the (uniform) thickness of the beam, β and k are the damping coefficients.

The following initial conditions reflect that the beam starts at rest and will not bent during motion:

$$u(x,0) = 0 = \frac{\partial}{\partial t}u(x,0).$$

Since the beam is fixed and clamped at one end, $x = 0$, we specify the boundary conditions as:

$$u(0,t) = 0 = \frac{\partial}{\partial x}u(0,t).$$

In addition, the following boundary condition assumes that the beam does not have shear stress at the free end, $x = L$:

$$\frac{\partial^3}{\partial x^3}u(L,t) = 0.$$

Finally, since the beam is laminated, each of the layers will expand at different rates when heated. This imbalance in the strains of the various layers creates a moment at the free end $x = L$ satisfying the following boundary condition:

$$\frac{\partial^2}{\partial x^2}u(L,t) = \Gamma\theta_{Al}(t), \quad (4)$$

which is linear with respect to the applied temperature.

3 Radial Basis Functions Method

Finite difference method and finite element method are widely adopted for the numerical modeling and simulation of the MEMS analysis. One of the major disadvantages of these traditional computational methods is their requirement on the generation of grids or meshes,

which hinders their application to solve high dimensional problems or problems under irregular domains. The rapid development of mesh-free methods during the last decade has recently overcome this mesh dependent disadvantage. There are basically two types of mesh-free methods: the Galerkin-based type that requires a background mesh, for instance, the smooth particle hydrodynamics method [Gingold and Moraghan (1977)], the diffuse element method [Nayroles, Touzot, and Villon (1992)], the hp-clouds method [Liszka, Duarte, and Tworzydlo (1996)], the Meshless Local Petrov-Galerkin [Atluri and Shen (2002)],[Atluri (2004)] the local boundary integral equation [Zhu, Zhang, and Atluri (1998)]; and the collocation-based type that does not require a background mesh, for instance, the Finite Point method [Onate, Idelsohn, and Zienkiewicz (1996)], the radial basis functions method [Chen, Ganesh, Golberg, and Cheng (2002); Kansa (1990a,b); Hon (2002); Hon and Schaback (2001); Shu and Yeo (2003, 2004); Wu and Shu (2002)], the method of particular solution [Chen, Muleshkov, and Golberg (1999); Golberg, Muleshkov, Chen, and Cheng (2003)] and fundamental solution [Chan and Chen (1996); Chen (1995a,b); Chen, Marcozzi, and Choi (1999)], the differential quadrature method [Bellman and Casti (1972); Shu and Richards (1992); Shu (2000); Wu and Liu (2000)] and the point interpolation methods [Liu (2003); Liu and Gu (2002)].

In this section, a numerical algorithm based on the Radial Basis Functions (RBFs) is developed for solving the governing equation (3) in the beam model subject to the given initial and boundary conditions. The idea of the RBFs method is to interpolate an unknown multivariate function $f(\mathbf{x}) \in \mathbb{R}^n$ by a linear combination of the radial basis functions $\phi(\| \mathbf{x}-\mathbf{x}_j \|)$:

$$f(\mathbf{x}) \simeq \sum_{j=1}^{N} \alpha_j \phi(\| \mathbf{x}-\mathbf{x}_j \|) + q_n^m(\mathbf{x}), \tag{5}$$

where $\mathbf{x}_j$ are N distinct data points in $\mathbb{R}^n$ and $q_n^m(\cdot)$ is a polynomial in $\mathbb{R}^n$ with degree up to $m-1$. Micchelli (1986) proved that when the N data points are all distinct, the resultant matrix for obtaining the undetermined coefficients α_j from a radial basis function interpolation is always invertible. A direct collocation is then performed by assuming that the representation (5) satisfies the given partial differential equations (3). From the boundary conditions, a unique set of the undetermined coefficients α_j is obtained by solving the resultant system of equations (refer to Franke and Schaback (1998) and Wendland (1999) for the theoretical foundation of this method).

In the computation of this paper, we choose $m = 0$ and $\phi = \| \mathbf{x}-\mathbf{x}_j \|^7$ to be the smooth spline of order 7.

3.1 Methodology

The beam model designed in the last Section 2 consists of the following partial differential equation (PDE):

$$a_1 \frac{\partial^2}{\partial t^2} u(x,t) + a_2 \frac{\partial}{\partial t} u(x,t) + \frac{\partial^4}{\partial x^4} u(x,t) = 0, \tag{6}$$

for $(x,t) \in [0,1]^2$ with initial conditions (of a resting beam)

$$u(x,0) = 0, \quad \frac{\partial}{\partial t} u(x,0) = 0, \tag{7}$$

and boundary conditions (at both ends of the beam)

$$u(0,t) = 0, \qquad \frac{\partial}{\partial t} u(0,t) = 0, \tag{8}$$

$$\frac{\partial^2}{\partial t^2} u(1,t) = \Theta(t), \qquad \frac{\partial^3}{\partial t^3} u(1,t) = 0, \tag{9}$$

where both the spatial and temporal variables, x and t, have been normalized. The parameters contained in (6) are related to those of the physical model (3) as

$$a_1 = \frac{L^4(\beta + \rho H)}{T^2 D}, \qquad a_2 = \frac{L^4 k}{TD}.$$

The source function in (9) corresponds to (4) as

$$\Theta(t) := L^2 \Gamma \overline{\theta}_{Al}(t).$$

To discretize equation (6) in time, we simply take a central difference approximation to the second partial order time derivative and a forward difference approximation to the first partial order time derivative of the function u to obtain:

$$\left[(a_1 + a_2 dt) u + dt^2 \frac{\partial^4}{\partial x^4} u \right] (x, t+dt) \tag{10}$$
$$= (2a_1 + a_2 dt) u(x,t) - a_1 u(x, t-dt),$$

where the fourth order spatial derivative of the function u is evaluating at time $t + dt$. This higher order spatial derivative will then be approximated by the radial basis functions as follow.

Given a set of data center $\{x_i\}_{i=1}^N$, the unknown solution $u(x,t+dt)$ of (10) is approximated by RBFs as:

$$u(x,t+dt) = \sum_{i=1}^{N} \alpha_i \phi_i(x), \tag{11}$$

where $\phi_i(x) = \phi(\|x-x_i\|)$ is a radial basis functions evaluated at data center x_i. Due to the differentiability of the smooth spline ϕ_i used as the RBFs in (11), the fourth order derivative of the unknown solution can be obtained by

$$\frac{\partial^4}{\partial x^4} u(x,t+dt) = \sum_{i=1}^{N} \alpha_i \frac{\partial^4}{\partial x^4} \phi_i(x).$$

Note that there are two boundary conditions on each side of the beam to be satisfied. Furthermore, these boundary conditions involve high order derivatives which normally cause numerical oscillation. The use of smooth spline of order 7 in our proposed method, however, does not encounter any oscillation problem.

For the choice of data centers $\{x_i\}_{i=1}^N$, we use the following function given in [Han and Liew (1999); Liew and Han (1997)] to place the first $N-4$ data centers:

$$x_i = \frac{1}{2}\left(1 - \cos\frac{(i-1)\pi}{N-5}\right), \quad i = 1,2,\ldots,(N-4), \tag{12}$$

in $[0,1]$. Following the idea of Liew, Teo, and Han (1999), we define the last four data centers $x_{N-3},\ldots,x_N$ to be $x_1 \pm \delta$ and $x_N \pm \delta$, where $\delta = \frac{1}{2}(x_2 - x_1)$, at each end of the beam to obtain the *final* set of N data centers. This choice of data set allows two extra degree of freedom to collocate the PDE and the second boundary condition imposed at both boundaries.

Collocating (6) at x_j for $j = 1,2,\ldots,N-4$ gives the following $N-4$ equations:

$$\sum_{i=1}^{N} \left[(a_1 + a_2 dt)\phi_i(x_j) + dt^2 \frac{\partial^4}{\partial x^4}\phi_i(x_j)\right] \alpha_i = (2a_1 + a_2 dt)u(x_j,t) - a_1 u(x_j,t-dt).$$

Further collocation at the four boundary conditions results in the following 4 equations:

$$\sum_{i=1}^{N} \alpha_i \phi_i(0) = 0, \qquad \sum_{i=1}^{N} \alpha_i \frac{\partial}{\partial x}\phi_i(0) = 0,$$

$$\sum_{i=1}^{N} \alpha_i \frac{\partial^3}{\partial^3 x}\phi_i(L) = 0, \qquad \sum_{i=1}^{N} \alpha_i \frac{\partial^2}{\partial^2 x}\phi_i(L) = \Theta(t+dt).$$

Parameter	ρH	D	Γ
Value	1.560E-3	10.442	4.755E-2
Parameter	Q	β	k
Value	3.774E7	1.3776E-3	123

Table 2 : Thermal properties of Al, SiO_2 and the surrounding Isopar fluid.

We now have a total of N equations for the N unknown coefficients α_i, $i = 1,2,\ldots,N$. Once these coefficients α_i have been obtained, the beam position is given by (11) at each time iteration. The time profile of the beam position is then obtained by iterating the solution process until $t = 1$.

4 Numerical Results

The solution of the heat equation (1) and boundary conditions (2) are used to determine $\theta_{Al}(t)$, and therefore $\Theta(t)$. This time dependent temperature is then imposed as a boundary condition in (9). The parameters' values used are listed in Table 2.

The numerical algorithm given in Section 3 is then used to compute the N coefficients α_i at each time iteration. We simply use $N = 21$ in our computation. For a $10\mu s$ heating pulse (see Figure 2), the time profile of the motion of the laminated beam is displayed in Figure 3. A comparison with the experimental data extracted from [Ross, Biswanger, Bohun, Bridge, Ling, Noel, Saujani, Spirn, and Ting (2000)] is also shown in Figure 4. It can be observed that the numerical result agrees extremely well with the experimental data. The maximum rate of deflection is about 0.2ms^{-1}.

To perform some parameters analysis, we assume that all parameters take the values listed in Table 2.

It is displayed in Figure 5 the dynamic responses of the beam at the free end to different values of applied currents, from $Q = 2E7$ to $10E7$, in the thermal equation (1). The numerical result verifies the direct relationship between the impulse and the amplitudes to the input currents. Note that the applied currents do not cause any apparent oscillation effect to the motion of the beam. This suggests that this numerical simulation can determine the maximum applicable current for a specify material from its fixed melting temperature.

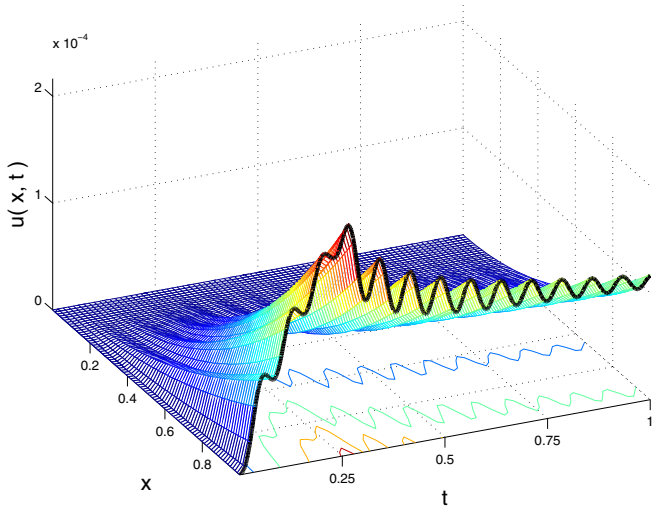

Figure 3 : Profile of the laminated beam motion for the $10\mu s$ ($t = 0.25$) heating pulse.

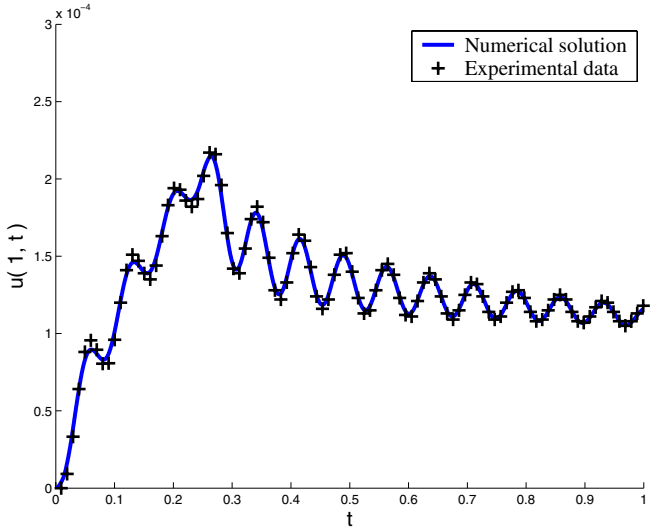

Figure 4 : Profile of the free end beam motion corresponding to Figure 3 and experimental data.

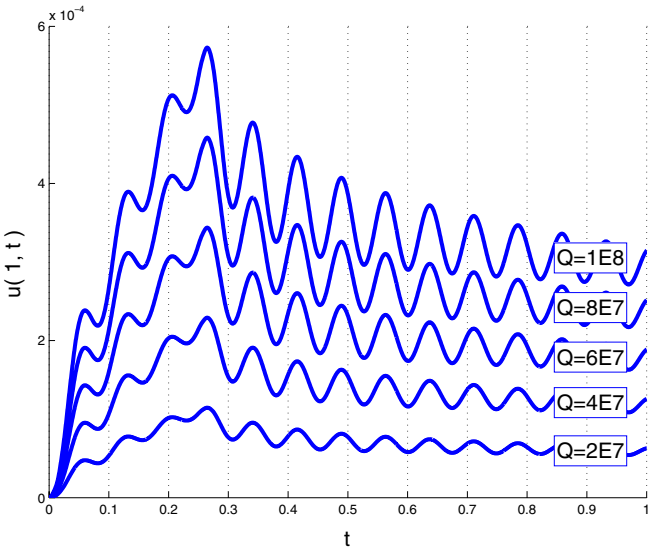

Figure 5 : Profile of the free end beam motion corresponding to different voltage Q.

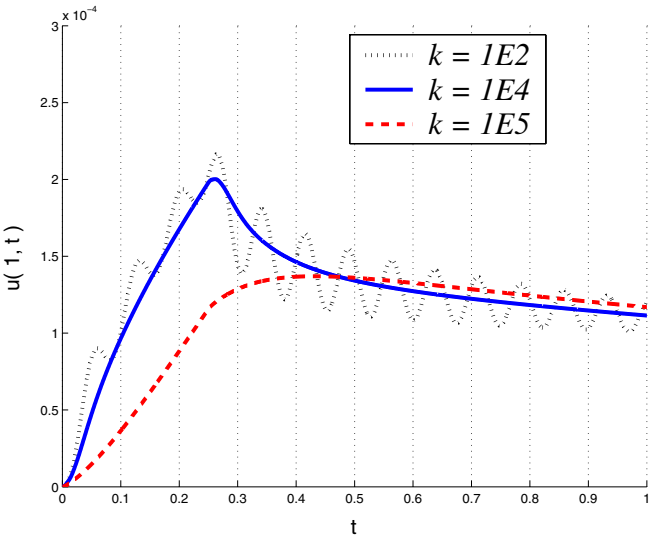

Figure 6 : Profile of the free end beam motion corresponding to different damping constant k.

Figure 6 shows the motion of the beam at the free end under different value of the damping constant k. As the friction increases, the deflection of beam decreases and does not oscillate. The critical damping occurs at $k^* \approx 4E{-}4$. This indicates that different thermal property of the isopar fluid surrounding the beam should be chosen according to the beam structure. In other words, an ideal isopar fluid will cause a "close-to-critical" damping effect to the beam.

Next, we vary the value of the composite mass $B = \beta + \rho H$. Figure 7 to Figure 9 show the deflection of the beam for $B = 5E{-}3$, $3E{-}3$, and $1E{-}3$, respectively. The numerical result indicates that a light (low composite mass) beam is more stable as it does not oscillate much. The numerical deflection of the beam under different value of the composite flexural rigidity D shown in Figure 10 to Figure 12 suggests that a soft (low rigidity) beam results in a higher rate of deflection, when com-

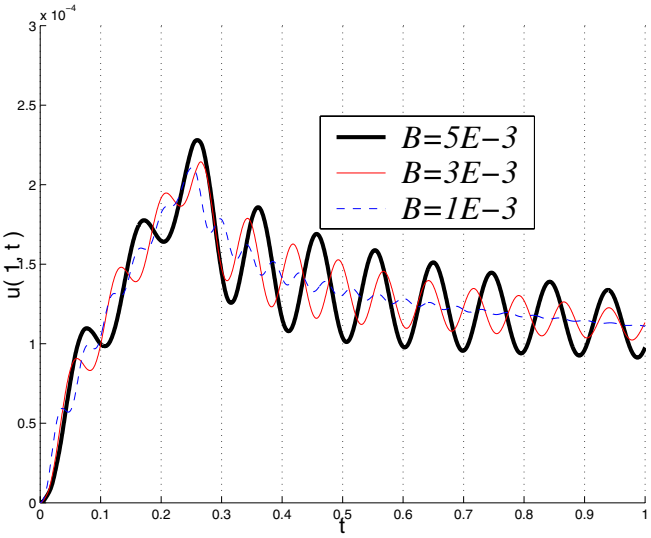

Figure 7 : Profile of the free end beam motion corresponding to composite mass $B = \beta + \rho H = 5E-1$.

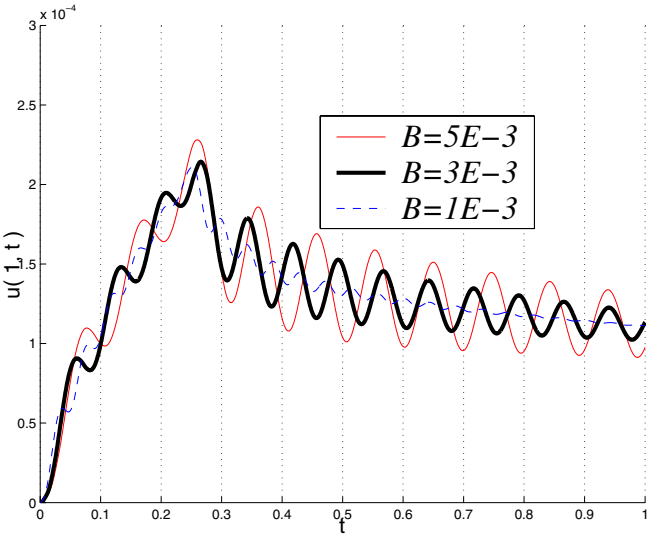

Figure 8 : Profile of the free end beam motion corresponding to composite mass $B = \beta + \rho H = 3E-1$.

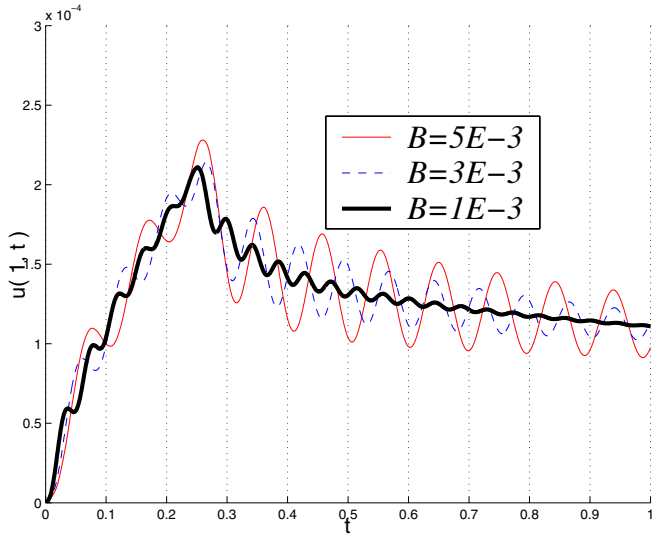

Figure 9 : Profile of the free end beam motion corresponding to composite mass $B = \beta + \rho H = 1E-1$.

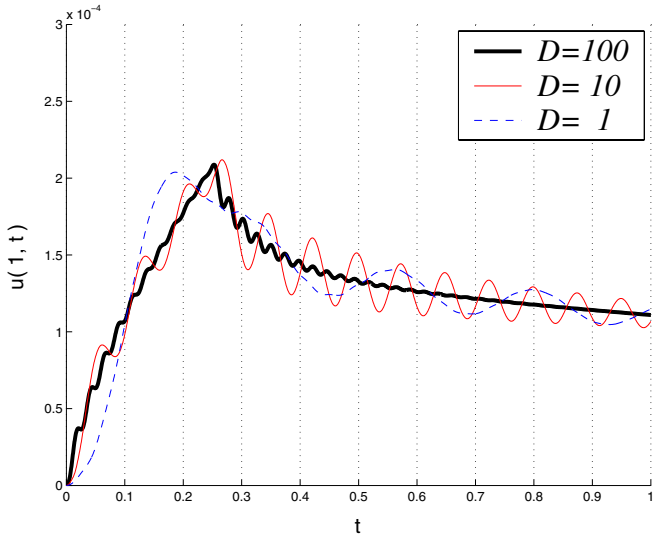

Figure 10 : Profile of the free end beam motion corresponding to composite flexural rigidity $D = 100$.

pared to a high rigidity one. These numerical simulations conclude that a lighter and softer beam is more preferable in controlling the inkjet printer to precisely deliver small ink droplets onto paper.

Finally, we assume that a second voltage pulse of $10\mu s$ is applied to the beam for another delivery of ink. Due to the thermal property of isopar fluid, the temperature of the beam cannot exceed 400K. The beam has to be cooled down after the first heating pulse. Once the heat supply to the beam has been turned off, the amplitude of the oscillation at the beam decreases as time increases. For numerical demonstration, we let the beam cool down for about $10\mu s$ (i.e., $t = 0.25$ in the normalized time) after the first $10\mu s$ heating pulse. The second pulse is then applied at $t = 0.51, 0.52, 0.53$, and 0.54 respectively. The resulting beam end motions are displayed in Figure 13. For better illustration, we also display respectively the zoom in figures of the starting and ending phases of the second deflection in Figure 14. The maximum rates of deflec-

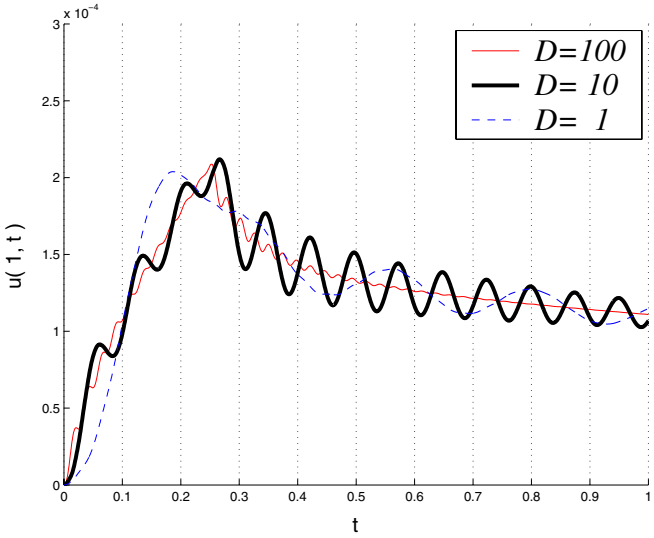

Figure 11 : Profile of the free end beam motion corresponding to composite flexural rigidity $D = 10$.

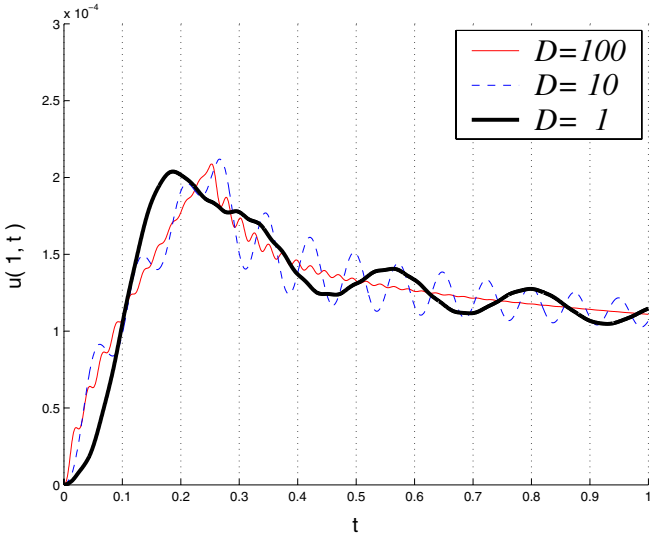

Figure 12 : Profile of the free end beam motion corresponding to composite flexural rigidity $D = 1$.

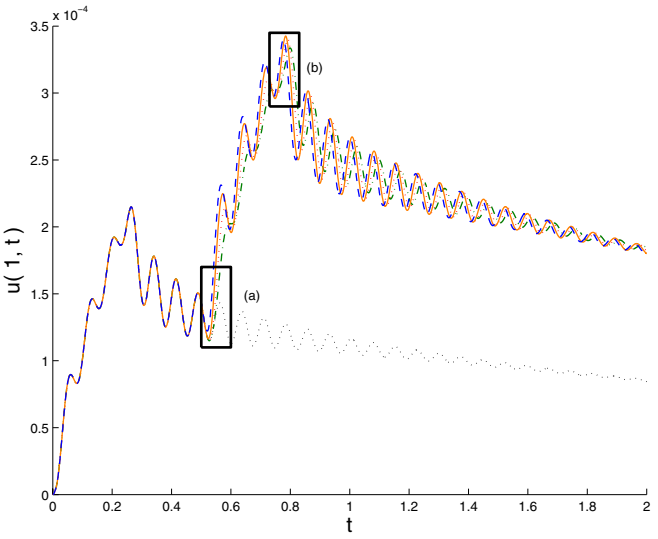

Figure 13 : Profiles of the free end beam motion for two $10\mu s$ heating pulses.

tion resulting from these second heating pulses are $+3\%$, $+5\%$, $+3\%$, and -2% respectively of the first heating pulse. This indicates that $t = 0.52$ is the best time to start the second pulse. The best time for the second current pulse is therefore the time when the beam reaches a local minima, which is expected from the understanding of the resonance phenomena.

5 Conclusion

In this paper we develop a computational method by using the radial basis functions, in particular, the smooth spline, for the numerical solution of a beam model arising from the studies of MEMS. In the model a free-end laminated beam composed to two materials, aluminum (Al) and silicon dioxide (SiO_2), was supplied with a voltage pulse of $10\mu s$ resulting at a temperature of about 400K and a maximum rate of deflection of about $0.2 ms^{-1}$. Numerical simulations with respect to different values of parameters are investigated. Simulated results show good match with the available experimental data. Furthermore, the numerical simulations indicated that an ideal construction of the laminated beam should be light in weight and low in rigidity. The surrounding isopar fluid (i.e., the ink) should be viscous enough to provide a close-to-critical damping effect to the beam. Finally, we predict that the optimal time for a second current pulse is the time when the beam reaches a local minima.

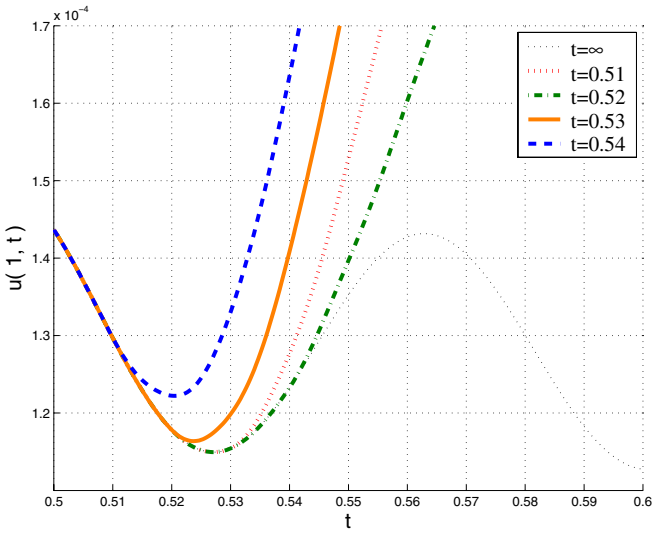

(a) Starting phase of deflection.

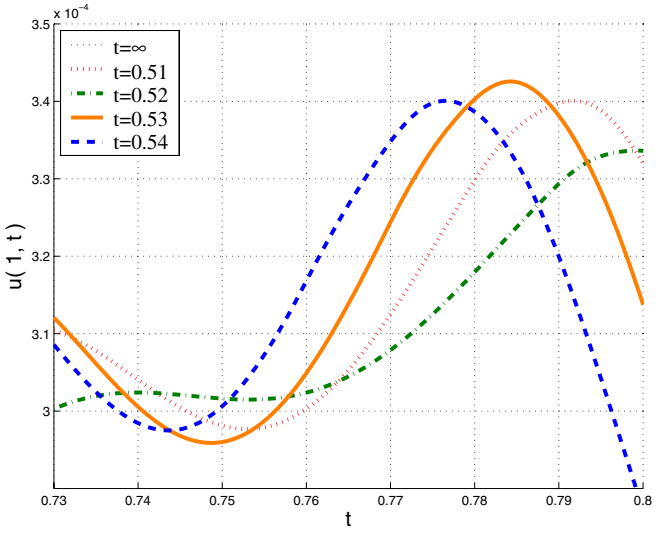

(b) Ending phase of deflection.

Figure 14 : Zoom in of Figure 13.

References

Atluri, S. N.; Han, Z. D.; Rajendran, A. M. (2004): A new implementation of the meshless finite volume method, through the MLPG "mixed" approach. *CMES: Computer Modeling in Engineering & Sciences*, vol. 6, pp. 491–514.

Atluri, S. N.; Shen, S. (2002): The meshless local Petrov-Galerkin (MLPG) method: a simple & less-costly alternative to the finite element and boundary element methods. *CMES: Computer Modeling in Engineering & Sciences*, vol. 3, no. 1, pp. 11–51.

Bellman, B., K.-G.; Casti, J. (1972): A technique for the rapid solution of nonlinear partial differential equations. *J. Comput. Phys.*, vol. 10, pp. 40–52.

Bochobza-Degani, O.; Nemirovsky, Y. (2002): Modelling the pull-in parameters of electrostatic actuators with a novel lumped two degrees of freedom pull-in model. *Sensors and Actuators A*, vol. 97-98, pp. 569–578.

Chan, C. Y.; Chen, C. S. (1996): Method of fundamental solutions for multi-dimensional quenching problems. In *Proceedings of Dynamic Systems and Applications, Vol. 2 (Atlanta, GA, 1995)*, pp. 115–121, Atlanta, GA. Dynamic.

Chen, C. S. (1995): The method of fundamental solutions and the quasi-Monte Carlo method for Poisson's equation. In *Monte Carlo and quasi-Monte Carlo methods in scientific computing (Las Vegas, NV, 1994)*, volume 106 of *Lecture Notes in Statist.*, pp. 158–167. Springer, New York.

Chen, C. S. (1995): The method of fundamental solutions for non-linear thermal explosions. *Comm. Numer. Methods Engrg.*, vol. 11, no. 8, pp. 675–681.

Chen, C. S.; Ganesh, M.; Golberg, M. A.; Cheng, A. H.-D. (2002): Multilevel compact radial functions based computational schemes for some elliptic problems. *Comput. Math. Appl.*, vol. 43, no. 3-5, pp. 359–378. Radial basis functions and partial differential equations.

Chen, C. S.; Marcozzi, M. D.; Choi, S. (1999): The method of fundamental solutions and compactly supported radial basis functions: a meshless approach to 3D problems. In *Boundary elements, XXI (Oxford, 1999)*, volume 6 of *Int. Ser. Adv. Bound. Elem.*, pp. 561–570. WIT Press, Southampton.

Chen, C. S.; Muleshkov, A. S.; Golberg, M. A. (1999): The numerical evaluation of particular solutions for Poisson's equation—a revisit. In *Boundary elements, XXI (Oxford, 1999)*, volume 6 of *Int. Ser. Adv. Bound. Elem.*, pp. 313–322. WIT Press, Southampton.

Collins, P.; Bradley, K.; Ishigami, M.; Zettl, A. (2000): Extreme oxygen sensitivity of electronic properties of carbon nanotubes. *Science*, vol. 287, pp. 1801–1804.

Endemano, A.; Desmuillez, M.; Dunnigan, M. (2002): System level simulation of a double stator wobble electrostatic micromotor. *Sensors and Actuators A*, vol. 99, pp. 312–320.

Franke, C.; Schaback, R. (1998): Solving partial differential equations by collocation using radial basis functions. *Appl. Math. Comput.*, vol. 93, no. 1, pp. 73–82.

Gingold, R.; Moraghan, J. (1977): Smoothed particle hydrodynamics: theory and applications to non-spherical stars. *Man. Not. Astrou. Soc.*, vol. 181, pp. 375–389.

Golberg, M. A.; Muleshkov, A. S.; Chen, C. S.; Cheng, A. H.-D. (2003): Polynomial particular solutions for certain partial differential operators. *Numer. Methods Partial Differential Equations*, vol. 19, no. 1, pp. 112–133.

Han, J.-B.; Liew, K. (1999): Static analysis of mindlin plates: the differential quadrature element method (dqem). *Computer Methods in Applied Mechanics and Engineering*, vol. in press.

Hon, Y. C. (2002): A quasi-radial basis functions method for american options pricing. *Comput. Math. Applic.*, vol. 43, pp. 513–524.

Hon, Y. C.; Schaback, R. (2001): On unsymmetric collocation by radial basis functions. *Appl. Math. Comput.*, vol. 119, pp. 177–186.

Huang, J. M.; Liew, K. M.; et al. (2001): Mechanical design and optimization of capacitive micromachined switch. *Sensors and Actuators A*, vol. 93, pp. 273–285.

Kansa, E. J. (1990): Multiquadrics—a scattered data approximation scheme with applications to computational fluid-dynamics. I. Surface approximations and partial derivative estimates. *Comput. Math. Appl.*, vol. 19, no. 8-9, pp. 127–145.

Kansa, E. J. (1990): Multiquadrics—a scattered data approximation scheme with applications to computational fluid-dynamics. II. Solutions to parabolic, hyperbolic and elliptic partial differential equations. *Comput. Math. Appl.*, vol. 19, no. 8-9, pp. 147–161.

Kim, P.; Lieber, C. (1999): Nanotube nanotweezers. *Science*, vol. 286, pp. 2148–2150.

Kovacs, G. (1998): *Micromachined Tranducers Sourcebook*. McGraw-Hill, New York.

Liew, K.; Han, J.-B. (1997): A four-node differential quadrature method for straight-sided quadrilateral reissner/mindlin plates. *Communications in Numerical Methods in Engineering*, vol. 13, no. 73-81.

Liew, K.; Teo, T.; Han, J.-B. (1999): Comparative accuracy of da and hdq methods for three-dimensional vibration analysis of rectangular plates. *Int. J. Numer. Meth. Engng.*, vol. 45, pp. 1831–1848.

Liszka, T.; Duarte, C.; Tworzydlo, W. (1996): Hp-meshless cloud method. *Computer Methods in Applied Mechanics and Engineering*, vol. 139, pp. 263–288.

Liu, G. R. (2003): *Mesh free methods*. CRC Press, Boca Raton, FL. Moving beyond the finite element method.

Liu, G. R.; Gu, Y. T. (2002): Boundary meshfree methods based on the boundary point interpolation methods. In *Boundary elements, XXIV (Sintra, 2002)*, volume 13 of *Int. Ser. Adv. Bound. Elem.*, pp. 57–66. WIT Press, Southampton.

Micchelli, C. A. (1986): Interpolation of scattered data: distance matrices and conditionally positive definite functions. *Constr. Approx.*, vol. 2, no. 1, pp. 11–22.

Nayroles, B.; Touzot, G.; Villon, P. (1992): Generalizing the finite element method: diffuse approximation and diffuse elements. *Computational Mechanics*, vol. 10, pp. 307–318.

Onate, E.; Idelsohn, S.; Zienkiewicz, O. (1996): A finite point method in computational mechanics: applications to convective transport and fluid flow. *Int. J. for Numerical Methods in Engineering*, vol. 39, pp. 3839–3866.

Ross, D.; Biswanger, K.; Bohun, C.; Bridge, L.; Ling, L.; Noel, D.; Saujani, S.; Spirn, D.; Ting, F. (2000): Optimal design of a micro-electrical-mechanical systems actuator. In *Report of the Third PIMS Graduate Industrial Math Modelling Camp*, pp. 16–23. Simon Fraser University, Pacific Institute for the Mathematical Sciences (PIMS).

Rueckes, T.; Kim, K.; Joselevich, E.; Tseng, G.; Cheung, C.; Lieber, C. (2000): Carbon nanotube-based nonvolatile random access memory for molecular computing. *Science*, vol. 289, pp. 94–97.

Shu, C. (2000): Differential quadrature and its application in engineering. London, Springer-Verlag.

Shu, C.; Richards, B. E. (1992): Application of generalized differential quadrature to solve two-dimensional incompressible navier-stokes equations. *Int. J. Numer. Meth. Fluids*, vol. 15, pp. 791–798.

Shu, C., D.-H.; Yeo, K. S. (2003): Local radial basis function-based differential quadrature method and

its application to solve two-dimensional incompressible navier-stokes equations. *Computer Methods in Applied Mechanics and Engineering*, vol. 192, pp. 941–954.

Shu, C., D.-H.; Yeo, K. S. (2004): Solution of partial differential equations by a global radial basis function-based differential quadrature method. *Engineering Analysis with Boundary Elements*, vol. 28, pp. 1217–1226.

Wendland, H. (1999): Meshless Galerkin methods using radial basis functions. *Math. Comp.*, vol. 68, no. 228, pp. 1521–1531.

Wu, T. Y.; Liu, G. R. (2000): The generalized differential quadrature rule for initial-value differential equations. *J. Sound Vibration*, vol. 233, no. 2, pp. 195–213.

Wu, Y. L.; Shu, C. (2002): Development of rbf-dq method for derivative approximation and its application to simulate natural convection in concentric annuli. *Comp. Mech.*, vol. 29, pp. 477–485.

Younis, M. I.; Abdel-Rahman, E. M.; Nayfeh, A. (2003): A reduced-order model for electrically actuated microbeam-based mems. *J. MEM Syst.*, vol. 12, no. 5, pp. 672–680.

Zhu, T.; Zhang, J.; Atluri, S. (1998): A meshless local boundary integral equation (lbie) method for solving nonlinear problems. *Computational Mechanics*, vol. 22, pp. 174–186.